ACADEMIA ROMÂNĂ
Revue Roumaine de Chimie
http://web.icf.ro/rrch/

Rev. Roum. Chim.,
2012, *57*(9-10), 877-889

MÖSSBAUER SPECTROSCOPY APPLIED TO SURFACES STUDY

Ion BIBICU

National Institute of Materials Physics, Bucharest-Măgurele, 105 bis Atomistilor street,
P.O. Box MG-7, PC 077125, Roumania, e-mail: bibicu@infim.ro

Received December 19, 2011

Mössbauer spectroscopy has (one of its most important features) the ability to simultaneously undertake bulk and surface analyses. It is a non-destructive technique that can be applied *in situ* to investigate surfaces of varying thickness using the secondary radiation emitted after resonant absorption of a gamma ray. A short description of the technique is presented. It allows a detailed analysis of the chemical state of Mössbauer atoms within the material, including valence state and chemical compound. Some applications of electron Mössbauer spectroscopy (CEMS), obtained in National Institute of Materials Physics are given. The experimental devices for surface studies are presented.

INTRODUCTION

Without a doubt, surface is the most important part of a solid. Wolfgang Pauli said that it was invented by devil.[1] Solid state physics applied to surfaces is a string of exceptions and special cases. The rule is that there are no rules. To make the problem even more complicated, interfaces are always present at surfaces. The most obvious one is the surface/bulk interface. Thus becomes clear why most of the experimental solid-state physics tools concentrate around surfaces.

The study of surfaces covers a very broad category of research topics and methods. The type of surface information recorded is controlled by the methodology used and typically involves an interaction between a selected probe and surface atoms. The researchers have varying opinions on the description of a surface, from a few atomic layers to may be 100 nm of the solid. Extending the application of surface techniques, one could include coatings which are microns in thickness, but which are usually thinner their substrates. Low energy particles such as electrons and neutrons are popular surface probes. Through interactions with the material a surface sensitive secondary probe may be emitted for detection. Such is the case in Mössbauer spectroscopy. In this paper is given a short presentation of the technique. Some applications of conversion electron Mössbauer spectroscopy (CEMS) are given. The experimental devices for surface studies are presented.

Mössbauer spectroscopy[2] (or nuclear γ resonance) is based on the incorporation of the emitting and absorbing nuclei within a solid matrix, which enables resonant recoil free absorption and emission of γ-rays. Its importance lies in the very narrow line width of the emitting photon resulting from the relatively long lifetime of the excited nuclear state – typically of 10^{-8} s, corresponding to a natural line width of the order of 10^{-8} eV – and the consequent ability to probe the variations in nuclear energy levels resulting from any discrete changes in the chemical state and/or environment of the Mössbauer nucleus. Such changes in nuclear energy levels are measured by modifying the energy of the probing γ-rays by applying a Doppler shift: a Mössbauer spectrum therefore consists of a plot of counts against applied Doppler velocity (positive and negative), the velocities corresponding to the addition and subtraction of Doppler energy shifts to the γ-ray energy. Significant recoil-free-fractions occur only for gamma energies less than 150 keV. For the

collecting data it is necessary to do measurements at low temperatures as the energy of the gamma ray increases. This fact obviously means that room or high temperature Mössbauer work is possible only for a limited number of elements, (*e.g.* ^{57}Fe, ^{119}Sn, ^{151}Eu).

Following resonant absorption of a gamma ray, the nucleus may de-excite by emission of a gamma ray or by the process of internal conversion where an inner (K or L) shell electron is emitted. Accompanying conversion electron emission is a characteristic X-ray emitted as a result of the repopulation of the inner energy levels. Detecting the three backscattered particles, permits surface studies to be performed. The electron signal is quite high for the ^{57}Fe and ^{119}Sn isotopes. In Fig. 1 is presented the disintegration scheme for ^{57}Co isotope and radiation delivered by ^{57}Fe isotope after interaction with 14.4 keV resonant, incident gamma rays. The ^{57}Fe isotope is the most studied isotope; over 60% from publications are dedicated to iron.

The normal transmission geometry investigates iron-containing samples of thickness typically < 30 microns. However, in scattering geometry surfaces, coatings and thin films can be studied on substrates and to various depths through the detection of three backscattered radiations. The maximum depths studied with ^{57}Fe isotopes are: 250 nanometers by 7.3 keV conversion electrons, (Conversion Electron Mössbauer Spectroscopy: CEMS) 20 microns by 6.4 keV X-rays, (X-ray Mössbauer spectroscopy: XMS) 30 microns by 14.4 keV gamma-rays (Gamma-ray Mössbauer spectroscopy GMS). The maximum depths studied with ^{119}Sn isotopes by conversion electron detection are up to 1000 nm. By means of the conversion electron detection, Mossbauer spectroscopy became one of the methods for surface characterization.

Mössbauer spectroscopy is studying the hyperfine interactions via the following hyperfine parameters:

a) Isomer shift *(σ)* arises because the nuclear energy levels are sensitive to changes in electron density at the nucleus, from differences in local topology as well as in valence state of the Mössbauer isotope. To a good approximation the isomer shift may be expressed as the difference between the transition energy of the absorber and the source.

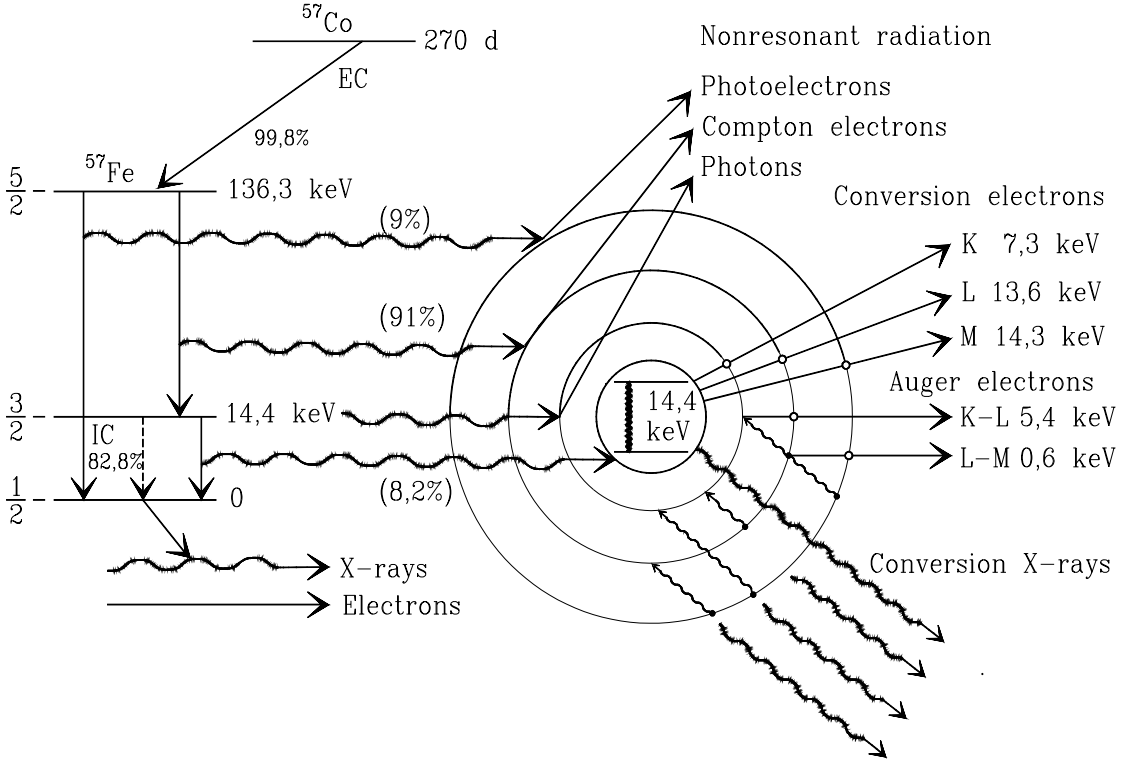

Fig. 1 – Resonance electron and conversion X-ray emission associated with nuclear gamma resonance for ^{57}Fe isotope.

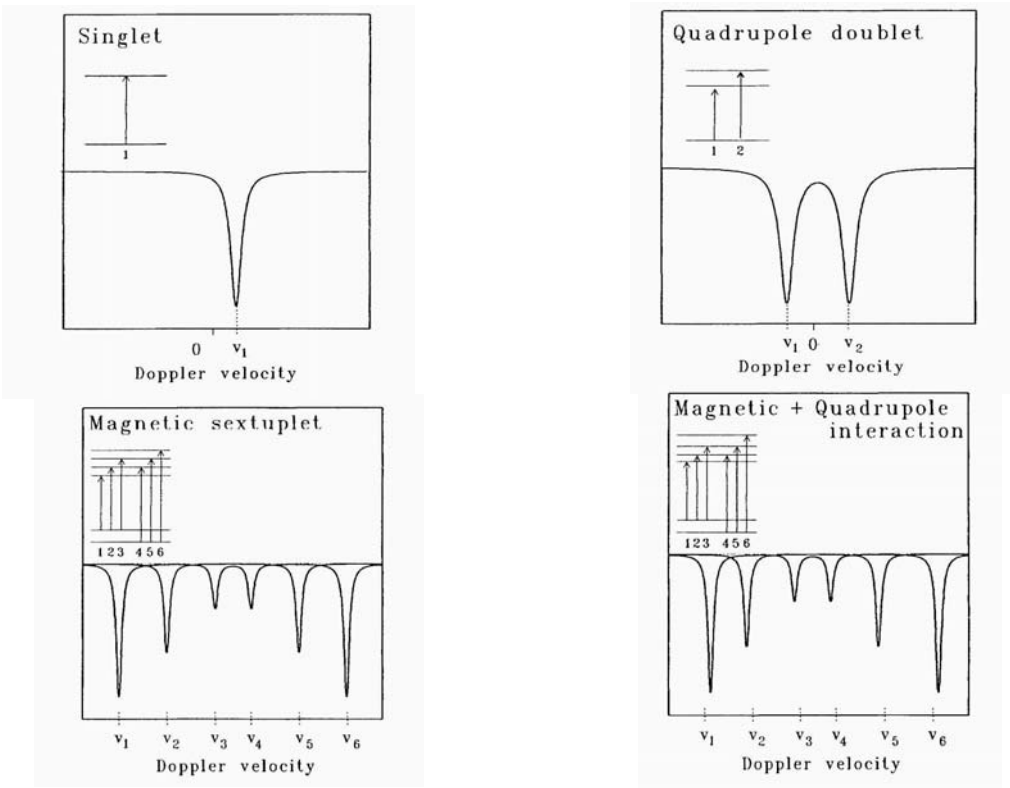

Fig. 2 – Mössbauer spectrum of ^{57}Fe isotope corresponding to: the isomer shift – singlet; the electric quadrupole splitting – quadrupole doublet; the magnetic hyperfine splitting – magnetic sextuplet; the case when electric quadrupole interaction is much smaller than magnetic interaction – magnetic and quadrupole interaction.

b) Electric quadrupole splitting *(ΔE_Q)* arises for any nucleus with nuclear spin quantum number I greater than 1/2 and which, therefore, possess a non-spherical charge distribution. The magnitude of this non-sphericity is given by the nuclear quadrupole moment Q, the sign of which depends on the shape of the deformation, *i.e.* whether the charge distribution is oblate or prolate about the nuclear spin axis.

c) Magnetic hyperfine splitting. This will occur if there is a magnetic field at the nucleus. The hyperfine magnetic field can originate either within the atom itself or as a result of placing the compound in an externally applied magnetic field. Any interaction between the nuclear magnetic dipole moment and hyperfine magnetic field at the nucleus lifts the degeneracy of the magnetic sublevels and gives rise to 2I + 1 levels. For iron, where I = 1/2 and 3/2, this results to a characteristic 6-line pattern. Separation between the peaks in the spectrum is proportional to the magnetic field at the nucleus. Measuring the magnetic hyperfine splitting permits to gain extremely useful information about the magnetic properties of the compounds investigated, information about directions of easy magnetization and strength of magnetic interactions. Particle size determination may also be made since the temperature at which magnetic ordering occurs depends critically on the particle size.

All mentioned hyperfine interactions, the corresponding spectra being given in Fig. 2 for ^{57}Fe isotope, can occur simultaneously. In magnetically ordered compounds, with a non-vanishing electric field gradient, the shape of the spectrum depends on the relative strengths of the magnetic dipole and the electric quadrupole interaction. A detailed analysis of the chemical state of Mössbauer atoms, within the material (valence state, chemical compound) is possible to be done from values of hyperfine interactions. The spectrum shape is a feature for a given chemical compound.

d) Recoil free fraction (f – factor). A necessary condition for absorption to occur is that the emitting and absorbing atoms form part of a rigid lattice, such that recoil energy associated with emission and absorption of the γ-quantum is taken by the lattice as a whole. The probability of such an event depends on the size of the recoil energy

and the spectrum of quantified vibration energy levels that describe the motion of the lattice. The intensity of the Mössbauer effect is thus determined by recoil free fraction or *f* factor $f = \exp(-k^2\langle x^2\rangle)$, where k is the wave number of the γ radiation ($k = 2\pi/\lambda$), $\langle x^2\rangle$ is the mean squared displacement of atoms from their average position due to lattice vibrations.

From values of hyperfine interactions and f-factor it is possible to derive the phase analysis and the site population for the various sites in a specific phase. Sometimes these hyperfine interactions might be time-dependent (diffusion, superparamagnetism and life-time). Additionally, the measuring efficiency might depend on the material and its temperature.

Mössbauer spectroscopy is one of the numerous methods for the analysis of the phase composition and the microstructure of materials. The ^{57}Fe is the most studied isotope followed by ^{119}Sn and ^{151}Eu. The three isotopes studied by us totalize more than 85% from publications.

Surfaces and interfaces require high sensitivity and selectivity. Mössbauer spectroscopy gains its sensitivity and selectivity from two factors: the penetration depth determined by the applied methodology and the isotopic specificity. Surface/interface information can be easily extracted from thin film or multilayer spectra by local character and the site specificity of Mössbauer spectroscopy, if the surface/interface atom contribution is meaningful.

Mössbauer spectroscopy[3-5] has as one of its most important features the ability to simultaneously undertake bulk and surface analyses. It is a non-destructive technique that can be applied *in situ* to investigate surface of varying thickness from thin films to coatings without the need to remove them from their substrate. On the other, it suffers from a lack of sensitivity and for the very thin surfaces and interfaces take too long acquisition times. With the growing interest in nanomaterials, catalysis and corrosion the surface Mössbauer technique will be more widely used.

EXPERIMENTAL

To observe the Mössbauer effect by detecting conversion electrons were used various magnetic and electrostatic spectrometers, parallel-plate avalanche counter, windowless electron multiplier, microchannel plate, channeltron and gas-filled proportional counters.[3] The proportional counter is the most used and it represents a cheap solution.

In our institute have been developed some proportional counters for conversion Mössbauer spectroscopy: detectors for conversion electron and transmission Mössbauer spectroscopy,[6,7] detector for conversion X-ray and transmission Mössbauer spectroscopy (CXMS),[8,9] detector assembly for simultaneous conversion electron, conversion X-ray and transmission Mössbauer spectroscopy,[7] versatile flow-gas proportional counter for surface Mössbauer spectroscopy,[10] All detectors are flow-gas type and operating at room temperature. Their construction permits for all detectors to realize simultaneous transmission and conversion measurements. The background due to photoelectrons is minimised by using low-Z materials as much as possible. The sample holder allows an easy manipulation of a sample, outside the detector and sample can always be repositioned in a reproducible manner with respect to the detector body. We have used for detectors an economical shielding which consists of a combination of lead, copper and steel disks. To destroy the characteristic radiation, alternate mounting of the lead, copper and steel disks were used. In order to absorb unfavourable KX-rays from the source, a plexiglas filter is placed in front of the shielding. We constructed flow-gas proportional counters for resonance electrons using two variants to dispose the anode wire: a circle around the sample,[6,7] and lines in front of the sample.[10] The second variant has better performance. The test measurements argue the versatility of these counters for the comparative study of surface and bulk properties of Mössbauer samples.

The proportional detector for conversion X-ray and transmission Mössbauer spectroscopy[8,9] has toroidal shape of the space detection and a lower efficiency for the 14.4 keV r-rays. The resonance effect can be optimised by a proper choice of the anode voltage and the filter. The design is simpler than those previously reported for similar devices.

The detector assembly for simultaneous conversion electron, conversion X-ray and transmission Mössbauer spectroscopy[7] consists mainly of two gas-flow proportional counters combined together. The sample to be studied is mounted inside the smaller counter designed for detecting electrons backscattered from the sample. The larger counter is used to detect conversion x-rays that come from the sample and pass through the electron counter. This assembly has a low efficiency for backscattered 14.4 keV y-rays. The counter design and operation are simpler than previously reported.

The versatile flow-gas proportional counter for surface Mössbauer spectroscopy[10] represents a synthesis of our experience in the development of flow-gas proportional detectors for surface studies. The main improvements obtained by new design are: the height of the detection volume can be changed in large limits from 1 to 38 mm, the detection volume can be chosen symmetrical or not in respect with anode plan, the anode changing is easily and different anode configuration can be used. By changing the volume detection and flow gas it is possible to make measurements by electron, X-ray detection or gamma-ray detection. The diagram of this detector is present in Fig. 3.

The detectors were inserted into a Mössbauer spectrometer. The spectrometric chain has been supplemented with additional modules such as to allow simultaneous recording of spectra. To test the performance of the counters, Mössbauer measurements were carried on reference samples as: a 25 μm thick stainless steel sample (type 310), a rhodium foil 30% enriched in ^{57}Fe, β-tin foil. The parameters of Mössbauer spectra have been calculated using a specialized, computer-fitting program, which assumes Lorentzian line resonances.

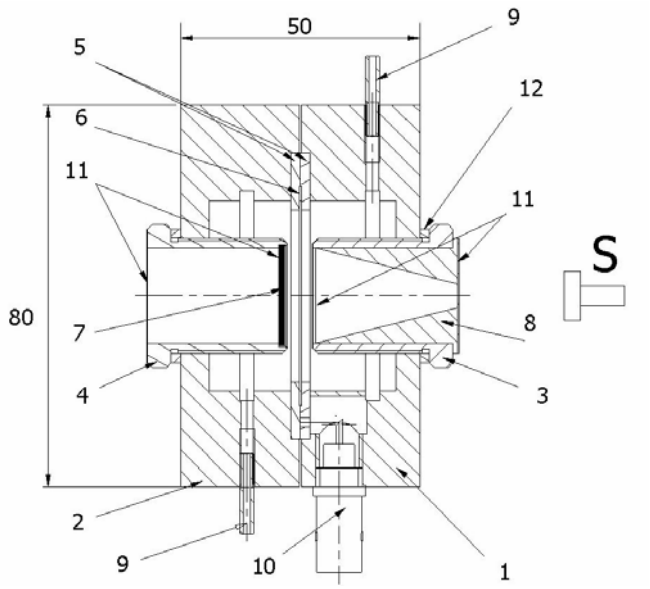

Fig. 3 – The cross section of the versatile flow-gas proportional counter, *1* and *2* main parts of the counter, *3* input piece, *4* sample holder, *5* teflon insulator, *6* anodic ring, *7* sample, *8* collimator, *9* gas connection, *10* high voltage connector, *11* mylar windows, *12* tightness piece, *S* Mössbauer source.

RESULTS AND DISCUSSION

In our institute were carried many studies by conversion electron Mössbauer spectroscopy (CEMS). So were investigated, for example: the effects induced, mainly in surface, by pulsed radio frequency annealing of $Fe_{81}B_{13.5}Si_{3.5}C_2$ (Metglass 2605 SC) glass,[11-14] the structural and magnetic properties of different films: $Fe_{81}B_{13.5}Si_{3.5}C_2$ films,[15] Fe-ion-implanted Cu and Ag films,[16] MnZnTi and NiZn ferrite films,[17] superficial characterization of α-iron oxides obtained by hydrothermal synthesis,[18] nanocrystallization of the $Fe_{87}Zr_6B_6Cu_1$,[19] corrosion processes,[20-30] the surface phase composition of bulk and thin films samples of $SnSe_2$,[31] etc. Some of them are shortly described below.

$Fe_{81}B_{13.5}Si_{3.5}C_2$ film

Mössbauer spectroscopy was used for structural investigation of laser ablated films of nominal composition $Fe_{81}B_{13.5}Si_{3.5}C_2$ starting from cast ribbon targets of Metglass 2605 SC.[11] The investigation of metallic glasses is of continuing interest in relation to their structural properties and potential applications. A plot of the room temperature CEMS spectra for both the film and the ribbon target is given in Fig. 4.[15] Both spectra exhibit the broadened six-line pattern corresponding to a distribution of the hyperfine fields at the Fe nuclei. An increase in the linewidth of the film spectrum is compatible with the average grain size decrease, which also causes broadening of X-ray diffraction lines. The lower value of 222.5 kOe, derived for the average hyperfine field of the deposited film (H_{film}), was related primarily to the structural changes following laser ablation of the material and not to a change in metalloid coordination of Fe atoms. The hyperfine field distributions indicate that the average hyperfine field for the thin film decreases on account of additional distribution in the low-field range. The effect was explained by assuming the contribution of nano-sized grains, which exhibit superparamagnetic behaviour, to the hyperfine field distribution. It was estimated, using a procedure given in literature, from the decrease in average hyperfine field at room temperature that the average size of the particles associated with the low-field distribution is about 15 nm. A simple deconvolution of the hyperfine field distribution for the thin film in a part that is identical to the ribbon distribution curve, and a low-field distribution, which can be assigned to nano-sized grains, allowed us, by measuring the areas under the two curves, to estimate a content of 23% Fe atoms embedded in nano-sized grains.

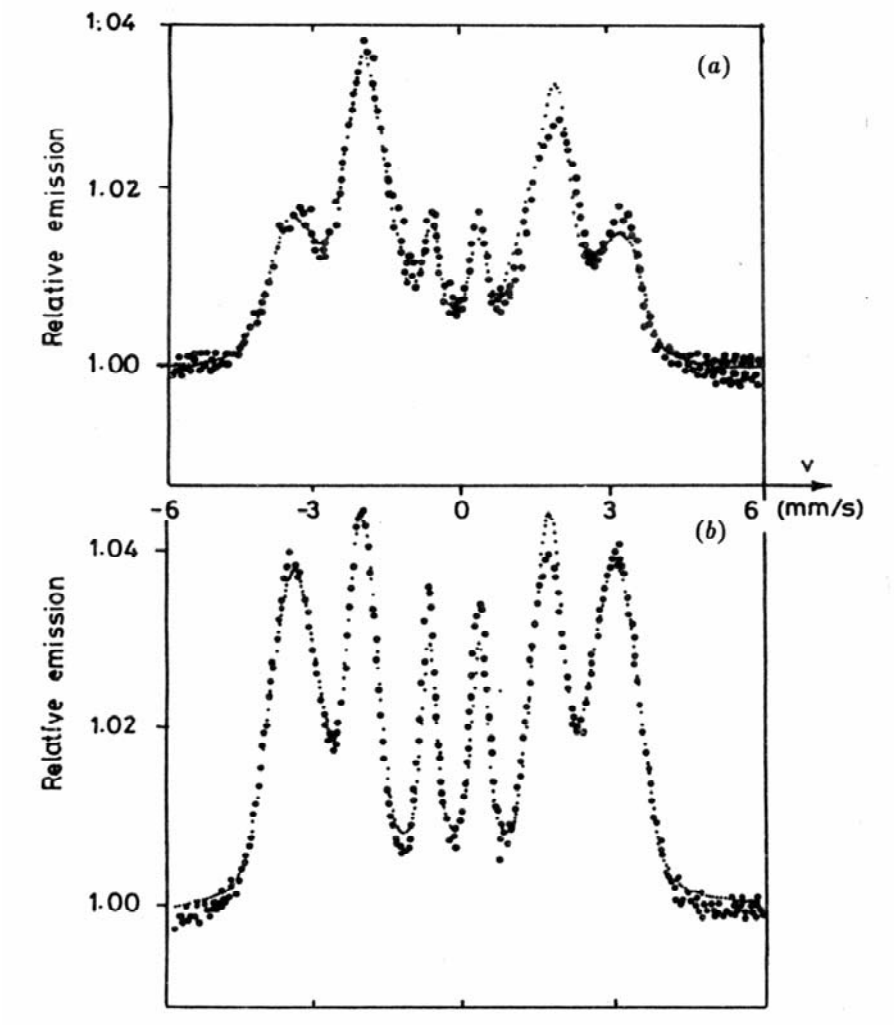

Fig. 4 – Room temperature CEMS spectra for both the (a) film and (b) the ribbon target of Metglass 2605 SC ($Fe_{81}B_{13.5}Si_{3.5}C_2$).

Fe-ion- implanted Cu and Ag films

Diluted granular films of Cu-Fe and Ag-Fe (iron content ≤ 2%) were produced using ^{57}Fe implantation Cu (Ag) films previously grown by laser ablation. The local structure of the implanted iron was evidenced by CEMS spectra analysis.[16] Fig. 5 shows the CEMS spectra recorded at room temperature where we separated two different (structural/aggregation) states of the implanted Fe. The singlets having isomer shifts at IS = 0.25 mm/s in Cu and 0.5 mm/s in Ag are likely to be due to individual Fe atoms dissolved in the FCC Cu or Ag matrices surrounded by 12 nearest-neighbour Cu (Ag) atoms. The large width suggests that Fe atoms be situated at damaged regions of the lattice. This appears as the dominant Fe phase in Fe/Cu film representing 85% of the total amount of iron in this film. For the Fe/Ag film this phase contributes only with 46% of the total iron amount. In fact, for the Fe/Ag film we observed an additional doublet in the CEMS spectrum, here assigned to iron atoms dissolved in Ag, but having one or more Fe atoms amongst its 12 nearest-neighbours. The presence of both Fe and Ag atoms in this shell destroys the cubic symmetry at the central iron site resulting in a large quadrupole splitting QS = 1.1 mm/s. From the relative intensity of the QS-doublet we estimate that 37% of the iron ions in Fe/Ag are in this non-symmetric phase. Thus, for the Fe/Ag film we obtain a relative content of 83% of iron atoms dissolved in the Ag matrix (therefore, in no ferromagnetic state) by summing the contributions from the singlet with 46% relative intensity and the doublet with 37% relative intensity. The presence of the quadrupole interaction in the silver matrix film also indicates a less packed structure that than of the copper matrix. Finally, the singlets at IS = − 0.13 mm/s in Fe/Cu and 0.08 mm/ in Fe/Ag have isomer shifts close to that of metallic iron and

hence are assigned to sufficiently large Fe clusters where each Fe atom has 12 Fe nearest neighbours as in the BCC structure of normal α-Fe. It was reasonable to assume that the six-line pattern expected from metallic iron is not seen here (our measurements were done at room temperature) because the Fe clusters exhibit superparamagnetic relaxation and the six-line pattern then collapses into a singlet. This metallic Fe phase has a relative intensity of 15% in the Fe/Cu film and 17% in the Fe/Ag film. These results were consistent with the data obtained magnetization and magnetoresistance measurements.

The corrosion of carbon steel in diluted ammoniacal media

Researchers have commonly ignored the industrial and residual waters containing ammonia/ammonium regarding them as non-dangerous in terms of corrosion. Relatively recent researches, however, have showed such waters have a negative impact on the environment leading to pipe corrosion in the cooling waters systems, especially in the ammonium fertilizer industry. The samples were corroded in a standard electrolytic cell with the followings diluted ammonia/ammonium solutions: diluted ammoniac solutions with NH_3 concentration of 10^{-1} M, 10^{-2} M, 10^{-3} M and 10^{-4} M,[20] ammonium salts solutions: 0.1M NH_4Cl, 0.1M NH_4Cl with 0.05M NH_4NO_3,[21] solution 10^{-3}M NH_3 with 510^{-3}M NH_4Cl.[22] The CEMS spectrum of the sample corroded in solution with 10^{-3} NH_3 concentration[20] is shown in Fig. 6. The best fit of the CEMS spectrum for the corroded sample uses an addition Fe^{3+} paramagnetic doublet respectively two paramagnetic doublets to the sextet.

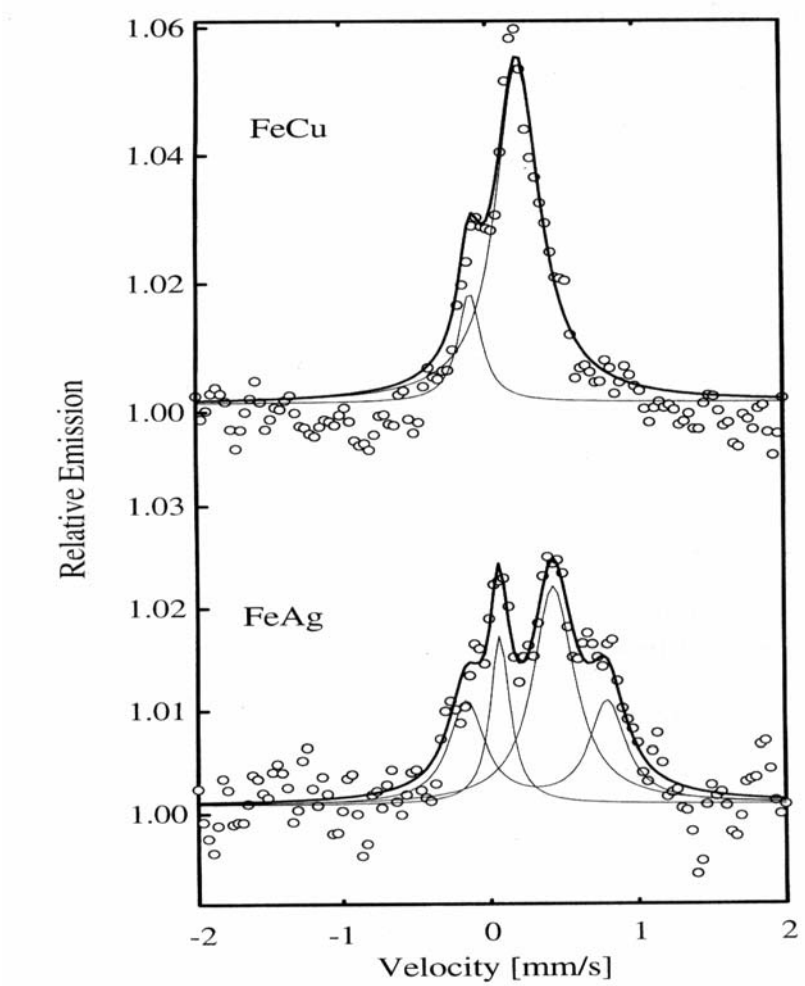

Fig. 5 – CEMS spectra of diluted granular films of Cu-Fe and Ag-Fe (iron content ≤ 2%) produced using ^{57}Fe implantation Cu (Ag) films, previously grown by laser ablation.

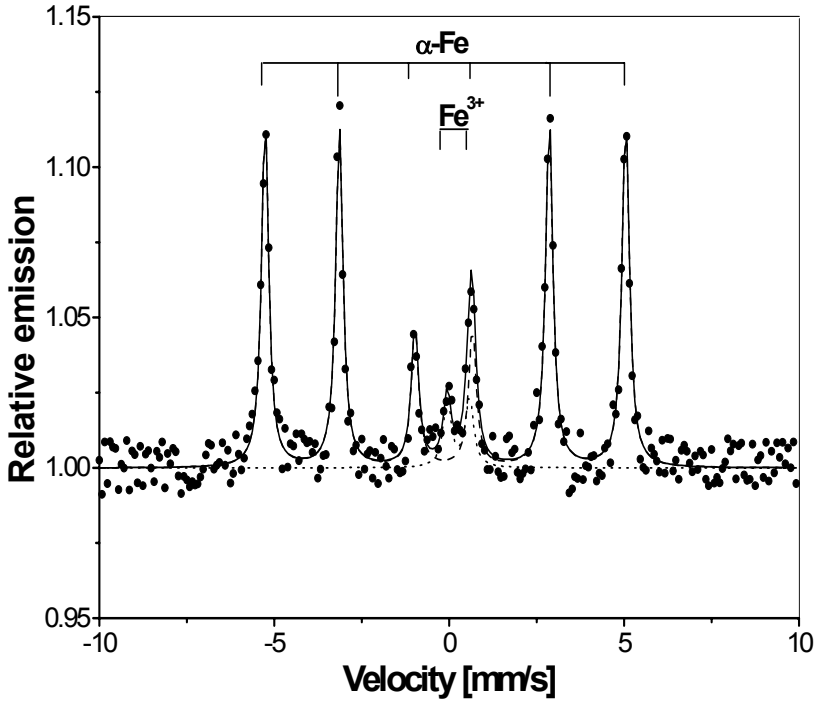

Fig. 6 – CEMS spectrum of a Fe-C steel sample corroded in a solution with 10^{-3} NH_3 concentration (• data; — fit; ··· Fe^{3+}; --- α-Fe).

The parameters of the sextet (hyperfine magnetic field, quadruple splitting, isomer shift, line width) are almost identical to those of the non-corroded sample. The slight changes of the hyperfine magnetic values and isomer shifts suggest that in the process of corrosion there may be a certain preference for the positions of iron, which are no close to the atoms of the alloying elements. The preferential orientation of the magnetic moments in the sample plane continues to exist even after the corrosion of the samples. The main difference between the corroded sample sextets and the non-corroded sextets consists in the decrease of the intensity lines corresponding to α-Fe. This demonstrates, once again, the presence of a superficial layer on the corroded samples surface. There is a process of inhibition of carbon-steel corrosion in the ammoniac solutions, which is evidenced by the increase of the superficial layer when NH_3 concentration decreases. The parameters of the doublets show the presence of Fe^{3+} and are similar to those shown by amorphous Fe^{3+} oxyhydroxides, superparamagnetic α-FeOOH and/or γ-FeOOH and Fe $(OH)_3$. Small relative area of the doublet, as well as its parameters shows the initial stage of the corrosion. At this stage we believe that the main product of the corrosion in NH_3 solution is an amorphous Fe^{3+} oxyhydroxide with a non-stoichiometric composition. Mössbauer data showed that for the samples corroded in ammonium salts solutions the main corrosion product is a mixture of Fe(III) ferrihydrate and FeOOH (alpha and/or gamma).The introduction of NO_3^- anion in a solution of 0.1M NH_4Cl in NO_3^-/Cl^- = 1/2 ratio has an inhibiting effect by decreasing the expansion rate of generalized corrosion of carbon steel. This effect is demonstrated by the increase of the sextet lines intensity and the dramatic decrease of the Fe^{3+} paramagnetic doublet.

Numerous advanced treatments using organic compounds have been proposed in order to improve the corrosion protection. The inhibition effect of three organic compounds: 2-mercapto-benzothiazol (MBT),[23] N-ciclohexil-benzothiazole-sulphenamida (NCBSA)[24] and etilentiouree (ETU)[25] on the corrosion of carbon-steel in diluted ammonia / ammonium solutions at room temperature were studied. The CEMS spectrum of a corroded sample in a solution with 10^{-3} HN_3 concentration with 250 ppm NCBSA inhibitor is presented in Fig. 7. The similar spectra are obtained for MBT and ETU inhibitors. In these spectra there is no evidence for any iron corrosion product at the surface.

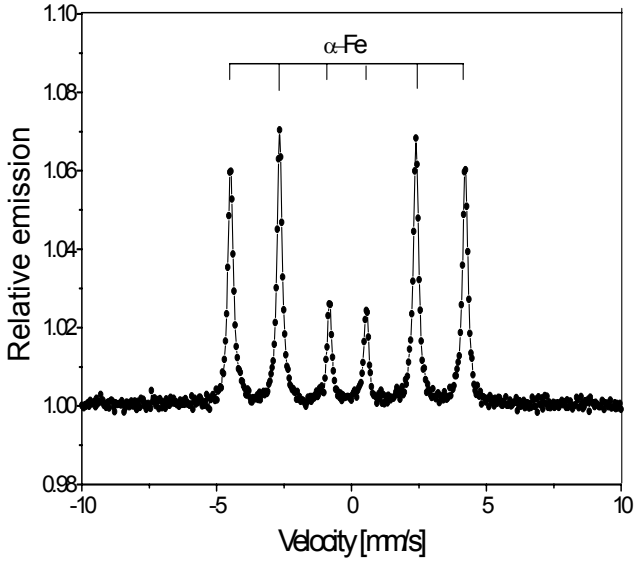

Fig. 7 – CEMS spectrum of a corroded sample in a solution with 10^{-3} HN_3 concentration with NCBSA inhibitor (● data; — fit; --- α-Fe).

In the spectrum there is no evidence for any iron corrosion product at the surface. A relative decrease of the α-Fe line intensities as compared with the sextet obtained in the corrosion process without inhibitor indicated formation of a superficial layer. Also the increased magnetic anisotropy of the CEMS spectra in the presence of the inhibitors confirms the action of the inhibitor. Mössbauer spectroscopy proved together other methods the inhibition action by a formation of a superficial film without iron compounds on the surface of the corroded samples. This layer is interpreted in terms of the formation of complexes between inhibitors and the metal cations present in the carbon-steel structure. The data indicate a good absorbability of inhibitor on the metal surface.

The corrosion of carbon steel in HCl solutions

Acid solutions are widely used in industry, the most important fields of application being acid pickling, industrial cleaning, acid decaling, oil-well acid in oil recovery and the petrochemical processes. One of the most aggressive media for the ferric materials is the aqueous solution of hydrochloric acid. To understand and to reduce the corrosive attack on metallic materials is an important task from economical point of view.

The samples were immersed in a closed system for 3h in solutions of 1 M HCl[21] or 2 M HCl.[27,28] The CEMS spectrum of the sample corroded in 1 M HCl solution is shown in Fig. 8. The best fit of the CEMS spectrum uses addition of two Fe^{3+} paramagnetic doublets to the sextet. The parameters of the doublets show the presence of Fe^{3+} and are similar to those shown by nonstoichiometric Fe^{3+} oxyhydroxides. The superficial layer consists of a mixture of α, β and γ-FeOOH. The superficial layer is thicker for sample corroded in HCl solutions then those corroded in ammonia media. In the 2 M HCl solution the corrosion layer is thicker than the layer formed in the corrosion in 1 M HCl solution and with the same superficial compounds.

The importance of inhibition is much greater in solutions of hydrochloric acid since iron and its alloys are the most exposed materials both in industrial and other media. The inhibition effect of five organic compounds for samples corroded in solutions of HCl solutions were investigated: ammonium polymolybdate (APM),[26] Fig. 9, n-acetyl p-aminobenzene sulfonamide (APAS),[27] N-(2hydroxybenzilidene) thiosemicarbazide (HBTC),[28] Bis (benzothiazolyl) disulphide (BTD)[29] and 2-(cyclohexylaminomercapto) benzothiazole (CMB).[30] All tested inhibitors operate in the same manner. The process of corrosion is considerable slown in the inhibitor presence and a superficial compound of Fe^{3+} without a magnetic arrangement is formed. The diminution of the corrosion process is indicates by the increased magnetic anisotropy of the CEMS spectra in the presence of the inhibitors. This means that the depth of the corroded surface layer is lower in the inhibitor presence or corrosion velocity diminished.

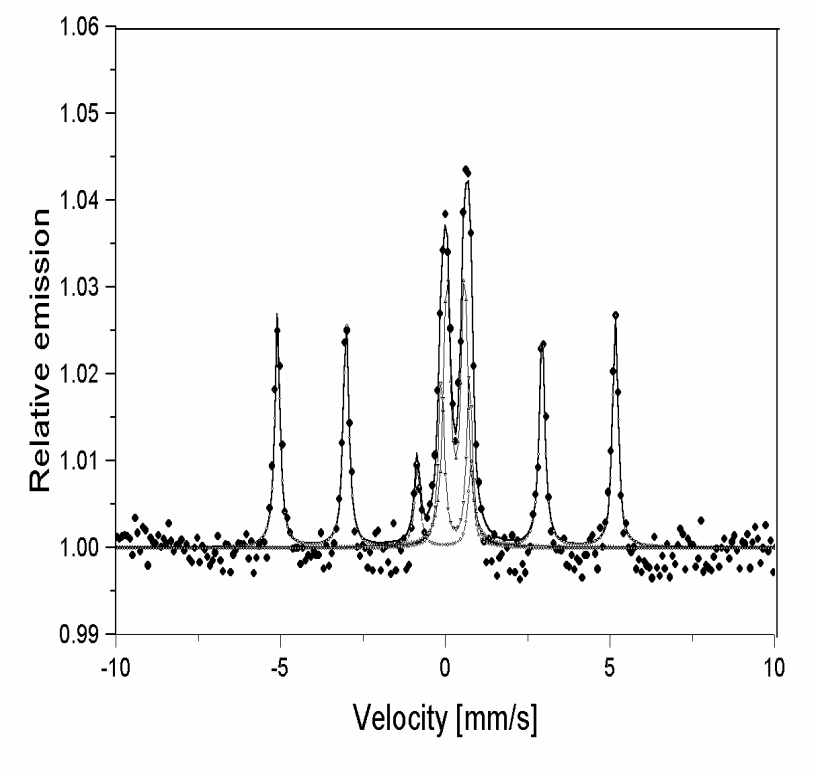

Fig. 8 – CEMS spectrum of a corroded sample
in a 1 HCl solution o (• data; — fit; -o- α-Fe; -Δ- doublet 1; -∇- doublet 2).

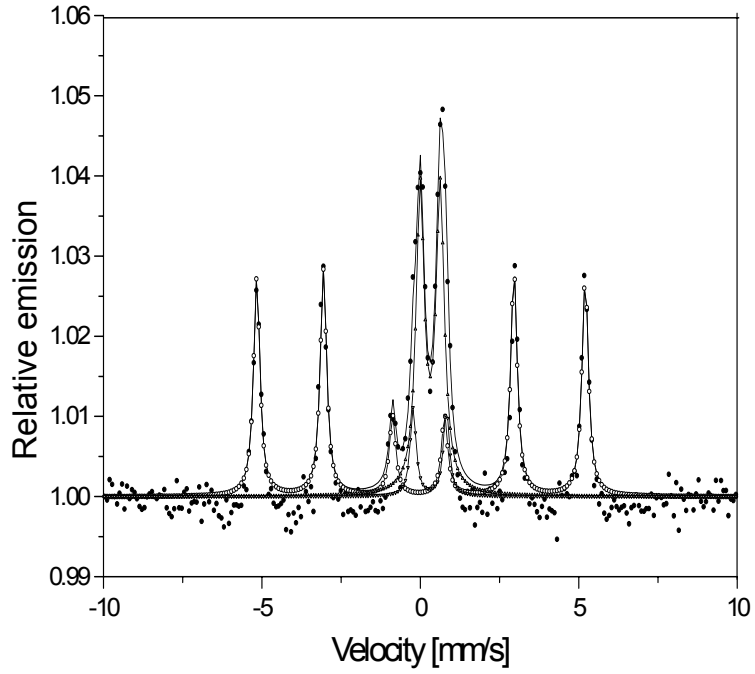

Fig. 9 – CEMS spectrum of a corroded sample in a 1M HCl solution
with APM inhibitor (• data; — fit; -o- α-Fe; -Δ- doublet 1; -∇- doublet 2).

By estimating the relative area of the superficial compound and the increased magnetic anisotropy of the CEMS spectra in the presence of the inhibitors, results that the compound has a smaller thickness or, in extreme case is similar with the layer formed in the corrosion process without inhibitor. The Mössbauer parameters of the compound in this case do not differ too large from

the ones found for the corroded sample in the solution without inhibitor. The new parameters can be ascribed to nonstoichiometric compounds as well as to low crystallinity, *e.g.* ferrihydrates. It is known that ferryhydrite is a precursor of other ordered iron oxyhydroxides. We consider that the organic inhibitors used in HCl solutions act as an incipient "rust transformer" and favours the formation of a "superficial closed layer". These inhibitors transform some constituents of rust into corrosion inhibiting oxide phases. For the corroded samples in a solution of 2M HCl, the inhibition process is the same as in 1M HCl solutions.

$SnSe_2$ (bulk and films)

Tin chalcogenides SnX_2 and SnX, where X=S, Se or Te, present a particular interest for their electronic properties and applications in gas sensors. They belong to amorphous and glassy chalcogenides, materials which are sensitive to light and other radiations. The state of tin in these materials is important for understanding of the sensing effect and improvement of the sensor performances, prepared from them. We have studied comparatively $SnSe_2$ bulk sample and films obtained from it by two methods.

The Mössbauer spectra obtained on $SnSe_2$ bulk sample by transmission Mössbauer spectroscopy and CEMS[31] are shown in Fig. 10. In Fig. 11 are presented the CEMS spectra obtained on $SnSe_2$ films deposited by two methods: pulsed laser deposition (PLD) and pulsed electron deposition (PED)[31].

The Mössbauer parameters for $SnSe_2$ bulk samples are closed to those given in literature for $SnSe_2$ and the line width values proves a well prepared compound. There is an oxidation process on its surface indicated by the presence of the SnO_2 oxide in the CEMS spectrum of the bulk sample. We consider an oxidation process in air atmosphere of the material. The thickness of thin films has been estimated to few nm.

The main component of the film spectra can be assigned to $SnSe_4$[31] species by its isomer shift values: 1.69 and 1.66 s. These species are known as tetrahedral Zintl anions [$SnSe_4$]. It is possible that studied films to be built from isolate $SnSe_4$ tetrahedra stabilized by atoms occupying intermediated positions. A similar process met in mesostructured chalcogenide-based materials with long-range order and semiconducting properties using molecular building blocks, linked by metal ions and surfactant molecules. The higher line width of the main component can be explained by the fact that $SnSe_4$ have tin environments slightly distorted from the basic tetrahedral symmetry.

The compound SnSe is present in both films in a small amount. The increased line width of the SnSe is explained by its quadrupole splitting with a value around 0.65 mm/s. The higher line width of the SnSe in the PLD film suggests a light structure distortion of the SnSe compound with orthorhombic structure. The SnSe presence can be explained by the occurrence of the reaction: $SnSe_2 \rightarrow SnSe + Se$ in the deposition process. In the film spectrum obtained by PLD deposition we identify a third component, assigned to SnO2 oxide. The oxide is localized at the film surface, the most probably, showing an oxidation in air atmosphere of the film.

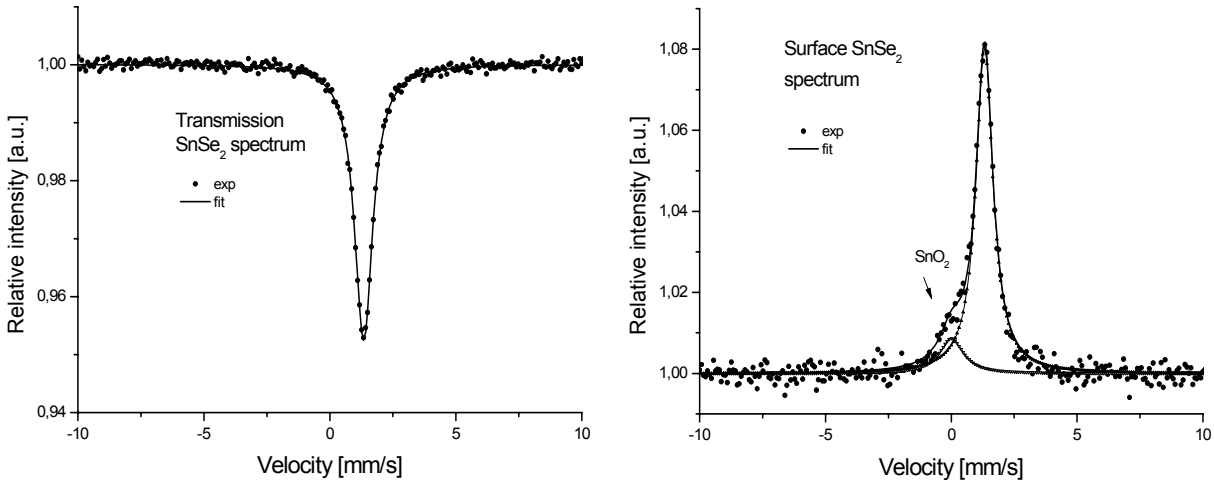

Fig. 10 – Spectra of $SnSe_2$ bulk sample obtained by TMS (left) and CEMS (right).

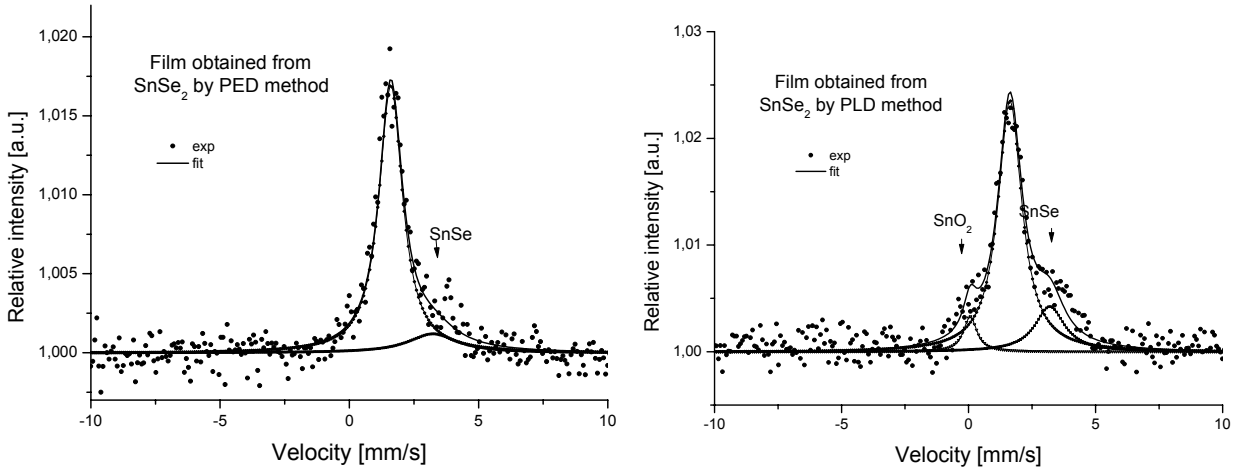

Fig. 11 – CEMS spectra of the films deposited from $SnSe_2$ by PED and PLD methods.

We believe, according to our results, that by PED deposition method a better film is obtained. The arguments for this affirmation are: a higher proportion of the main component, a lower line width of the main component, a lower line width of the SnSe component, the absence of the SnO_2 oxide.

CONCLUSIONS

We proved the possibility to make superficial measurements in the nano or micro range by Mössbauer spectroscopy using ^{57}Fe and ^{119}Sn Mössbauer isotopes. Measurements were made with different flow gas detectors in a backscattering geometry by detection of electron or X rays.

Surface measurements were realized on the following samples: $Fe_{81}B_{13.5}Si_{3.5}C_2$ (Metglass 2605 SC) glass, $Fe_{81}B_{13.5}Si_{3.5}C_2$ films, Fe-ion-implanted Cu and Ag films, MnZnTi and NiZn ferrite films, α-iron oxides obtained by hydrothermal synthesis, $Fe_{87}Zr_6B_6Cu_1$, carbon steel corroded in diluted ammoniacal media or HCl solutions in presence or absence of organic corrosion inhibitors, β-tin foil, bulk and thin films samples of $SnSe_2$.

Acknowledgements: This work was supported by National Authority for Scientific Research (ANCS) under Core Program Project PN09-45 and CNCSIS-UEFISCSU, Roumanian project PNII-IDEI, 4/2010, code ID-106.

REFERENCES

1. A. Zangwill, "Physics at Surfaces", Cambridge University Press, Cambridge, 1988.
2. R. L. Mössbauer, *Z. Physik*, **1958**, *151*, 124-143.
3. G. N. Belozerskii, "Moessbauer Studies of Surface Layers, (Studies in Physical and Theoretical Chemistry Series; 81)", Elsevier Science, Oxford, 1993.
4. G. J. Long and F. Grandjean, (Eds.), "Moessbauer Spectroscopy Applied to Magnetism and Materials Science", vol. 2, Plenum, Dordrecht, 1996.
5. A. G. Maddock, "Moessbauer Spectroscopy: Principles and Applications of the Techniques", Horwood Chemical Science Series, Horwood, Chister, 1997.
6. I. Bibicu, M. S. Rogalski, Gh. Voiculescu, G. Nicolescu and D. Barb, *Rev. Roum. Ph*ys., **1992**, *37,* 315-317.
7. I. Bibicu, M. S. Rogalski and G. Nicolescu, *Meas. Sci. Technol*., **1996**, *7*, 113-115.
8. I. Bibicu, M. S. Rogalski and G. Nicolescu, *Nucl. Instrum. Methods Phys. Res. B*, **1994**, *94*, 330-332.
9. I. Bibicu and M. S. Rogalski, *J. Phys. III*, **1994**, *4*, 2495-2499.
10. I. Bibicu, G. Nicolescu and C. Cretu, *Hyperfine Interact.*, **2009**, *192,* 85-91.
11. M. Rogalski and I. Bibicu, *Mater. Lett.*, **1992**, *13*, 32-34.
12. I. Bibicu, M. S. Rogalski and G. Nicolescu, *Phys. Stat. Sol. (b),* **1993**, *178*, 459-464.
13. M. S. Rogalski, I. Bibicu and M. Sorescu, *Hyperfine Interact.*, **1994**, *92*, 1317-1321.
14. M. S. Rogalski and I. Bibicu, *Physica Stat. Sol (b)*, **1996**, *195*, 531-536.
15. M. S. Rogalski, T. J. Jackson, I. Bibicu and S. B. Palmer, *J. Phys. D Appl. Phys.*, **1994**, *27*, 2167-2170.
16. M. M. Pereira de Azevedo, J. B. Sousa, J. A. Mendes, B. G. Almeida, M. S. Rogalski, Yu. G. Pogorelov, I. Bibicu**,** L. M Redondo, M. F. da Silva, C. M. Jesus, J. G. Marques and J. C. Soares, *J. Magn. Magn. Mater.*, **1997**, *173*, 230-240.
17. M. M. Amado, M. S. Rogalski, L. Guimaraes, J. B. Sousa, I. Bibicu, R. G. Welch and S. B. Palmer, *J. Appl. Phys.*, **1998**, *83,* 6852-6854.
18. L. Diamandescu, D. Mihaila-Tarabasanu, N. Popescu-Pogrion, A. Totovana and I. Bibicu, *Ceram. Int.*, **1999**, *25*, 689-692.
19. I. Bibicu, S. Garitaonandia, F. Plazaola and E. Apinanz, *J. Non-Cryst. Solids*, **2001**, *287*, 277-281.
20. I. Bibicu, A. Samide and M. Preda, *Mat. Lett.*, **2004**, *58,* 2650-2653.

21. A. Samide, I. Bibicu, M. Rogalski and M. Preda, *J. Radioanal. Nucl. Chem.*, **2004**, *261*, 593-596.
22. A. Samide, I. Bibicu, B. Tutunaru and M. Preda, *Rev. Chim-Bucharest*, **2005**, *56,* 850-853.
23. A. Samide, I. Bibicu, M. Rogalski and M. Preda, *Acta Chim. Slovenica*, **2004**, *51*, 127-136.
24. A. Samide, I. Bibicu, M. S. Rogalski and M. Preda, *Corros. Sci.*, **2005,** *47,* 1119-1127.
25. A. Samide, I. Bibicu, M. Rogalski and M. Preda, *Rev. Chim-Bucharest* , **200**3, *54,* 927-931.
26. A. Patru, I. Bibicu, M. Agiu, M. Preda and B. Tutunaru, *Mater. Lett.*, **2008**, *62*, 320-322.
27. A. Samide, I. Bibicu and E. Turcanu, *Rev. Chim-Bucharest* , **2009**, *60,* 564-567.
28. A. Samide, I. Bibicu and E. Turcanu, *Chem. Eng. Commun.*, **2009**, *196*, 1008-1017.
29. A. Samide and I. Bibicu, *Rev. Roum. Chem.*, **2009**, *54,* 33-43.
30. A. Samide and I. Bibicu, *Surf. Interface Anal.*, **2008**, *40*, 944-952.
31. I. Bibicu, A.Lőrinczi, A.Velea, F. Sava and M. Popescu, *Optoelectro. Adv. Mater. – Rapid Commun.*, **2010**, *4,* 1568-1571.